Mine Water Environ (2017) 36:479–494
DOI 10.1007/s10230-017-0454-4

TECHNICAL ARTICLE

Pyrite Weathering in Reclaimed Shale Overburden at an Oil Sands Mine near Fort McMurray, Canada

Willemijn M. Appels[1,2] · Susan N. Wall[3] · S. Lee Barbour[4] · M. Jim Hendry[3] · Craig F. Nichol[5] · Saidur R. Chowdhury[6]

Received: 5 August 2016 / Accepted: 26 April 2017 / Published online: 3 May 2017

Abstract Saline-sodic shale overburden associated with oil sand mining is a potential source of salt release to surface water and groundwater and can lead to salinization and/or sodification of reclamation covers. Weathering of shale overburden due to oxidation of sulphide minerals within the shale leads to sulphate (SO_4^{2-}) production and increased salinity. The controls on the rates of weathering of a shale overburden dump in the oil sands region of northern Alberta were determined from soil chemistry sampling and in situ monitoring of pore gases (O_2, CO_2, CH_4) in three shallow profiles (1.9–4.45 m deep) and one deep (25 m deep) profile under reclamation covers of varying thickness. Oxidation, defined by the depth over which O_2 concentrations were depleted, reached depths of approximately 1.1 m under the reclamation soil covers over a 6 year period after dump placement. Calculations of SO_4^{2-} production rates and weathering depths were consistent with numerical simulations of the diffusion and subsequent consumption of atmospheric O_2 in the overburden. The rate of SO_4^{2-} production during the 6 year weathering period estimated from direct measurements of solids chemistry ranged from 0.70 to 8.3 g m^{-2} day^{-1}. The rates calculated from the oxygen diffusion models were within that same range, between 1.6 and 4.1 g m^{-2} day^{-1}.

Keywords Pyrite oxidation · Oxygen diffusion · Overburden dump · Oil sands · Reclamation

✉ Willemijn M. Appels
willemijn.appels@gmail.com

1 Global Institute for Water Security, University of Saskatchewan, 11 Innovation Blvd, Saskatoon, SK S7N 3H5, Canada

2 Present Address: Lethbridge College, 3000 College Dr S, Lethbridge, AB T1K 1L6, Canada

3 Department of Geological Sciences, University of Saskatchewan, 114 Science Place, Saskatoon, SK S7N 5E2, Canada

4 Department of Civil and Geological Engineering, University of Saskatchewan, 57 Campus Drive, Saskatoon, SK S7N 5E9, Canada

5 Deparment of Earth and Environmental Sciences, University of British Columbia, 1177 Research Rd, Kelowna, BC V1V 1V7, Canada

6 Toronto Inspection Ltd, 110 Konrad Crescent, Markham, ON L3R 9X2, Canada

Introduction

Surface mining generates large volumes of overburden waste (Amos et al. 2015). In the Athabasca oil sands region of northern Alberta, about 4800 km^2 of oil sands reserves are potentially extractable by surface mining of bitumen (Government of Alberta 2016). The oil sand deposits are covered by Holocene organic material (peat), Quaternary glacial deposits, and up to 75 m of Cretaceous Clearwater formation that is dominated by uncemented clay-shales, clay-silts, fine-grained sands, and several thin indurated sandstone layers. The Clearwater shale deposits in the Athabasca oil sands region are of marine origin and contain substantial amounts of pyrite (Gautier 1986; Haug et al. 2014; Mermut and Arshad 1987). The excavation and placement of these deposits into large overburden dumps exposes these deposits to oxygen and induces subsequent weathering of the pyrite. In conventional mine waste rock piles, oxidation of sulphide minerals such as pyrite generates acid mine drainage (AMD; e.g. Emrich and Merritt 1969; Lefebvre et al. 2001a; Lottermoser 2010; Nordstrom 2011; Sracek et al. 2004). However, in the case of

oil sands overburden shales, carbonate minerals (e.g. calcite, dolomite, and siderite) are present, which can buffer the acidity (Haug et al. 2014). The resultant H_2CO_3 can further dissociate to bicarbonate (HCO_3^-) or water (H_2O) and carbon dioxide (CO_2). The release of Ca^{2+} can result in ion exchange at the exchange sites of clay minerals with a concomitant increase in Na^+ in the pore water (Hendry et al. 1986). Ca^{2+} can also react with the SO_4^{2-} and water to form gypsum ($CaSO_4 \cdot 2H_2O$).

In the case of the oil sands' saline-sodic overburden mine waste, the primary risk associated with pyrite oxidation is the generation of high concentrations of dissolved ions such as Na^+ and SO_4^{2-}, which can be transported into reclamation cover soils and cause salinization and/or sodification of reclamation soil profiles or adjacent wetlands (Kessler et al. 2010; Olatuyi and Leskiw 2014). Field studies at a reclaimed shale overburden dump in the Athabasca oil sands region north of Fort McMurray, AB, Canada showed that salts had migrated upward into the soil reclamation covers (Hilderman 2011; Huang et al. 2015b; Kessler et al. 2010). There is evidence that the mobilized salts in the upper overburden are flushed by net percolation into the dump and subsurface flow along the interface between the soil and overburden (Kelln et al. 2007, 2008, 2009); however, the rates and duration of oxidation in the reclaimed dumps that contribute to this salinization of the overlying soil remain poorly quantified.

The present study focused on a large reclaimed overburden shale dump at an oil sands mine in northern Alberta, Canada. The objectives were twofold: first, to define the characteristic depths and rates of the dominant weathering mechanisms in the shale overburden dump and second, to quantify how these vary as a function of location on the dump and depth of the reclamation cover. These objectives were attained by collecting profiles of soil geochemistry and in situ pore gas composition within the overburden shale deposit, and by modeling the rates of O_2 diffusion and consumption in the overburden shale.

Study Site

This study was conducted at a reclaimed overburden dump at the Mildred Lake mine operated by Syncrude Canada Ltd., 40 km north of Fort McMurray, Alberta, Canada (Fig. 1). The climate of the region is sub-humid, continental with cold winters and warm summers. The average yearly precipitation is 417 mm (1952–2011), of which 106 mm occurs as snow (Huang et al. 2015a, b). Potential evapotranspiration is 517 mm per year (1999–2009) (Huang et al. 2015a, b). The oil sand deposits at this mine are overlain by 50–75 m of saline-sodic Cretaceous shale of the Clearwater formation. The Clearwater formation has an average grain size distribution of 6.5% sand, 53.0% silt, and 40.5% clay (Chapman 2008) and is characterized as glauconitic silty sands with light to dark gray clay silts dominated by smectite clays (Chapman 2008; Spiers et al. 1984).

The study site, referred to as South Bison Hill (SBH; Fig. 1), was constructed by a combination of end or push dumping into a mined out pit followed by free dumping in approximately 5 m lifts over the top 40 m of the dump (Boese 2003; Chapman 2008). The dump was constructed between 1980 and 1996 with approximately 100 Mm^3 of overburden placed over approximately 2 km^2 (depth range 50–90 m). The dump is dominated by saline-sodic shale, with traces of low-grade lean oil sands and small amounts of glacial till, as well as unevenly distributed cobblestones and boulders (Chapman 2008). The dump was contoured into several discrete watersheds in 1998 and 1999 and capped with two-layer reclamation soil covers consisting of salvaged glacial till topped with a mixture of peat and glacial till. Geotechnical characteristics and soil hydraulic properties of these materials are presented in Table 1. Three 200×50 m research watersheds were constructed along the north-facing slope using three different soil cover alternatives of the aforementioned materials (Fig. 1b). The D1 cover was 30 cm of till covered by 20 cm of a peat-mineral mixture; the D2 cover was 20 cm of till covered by 15 cm of peat-mineral mixture; while the D3 cover was 80 cm of till covered by 20 cm of the peat-mineral mixture. On the plateau of the dump, the soil cover is nominally 120 cm thick with 100 cm of till overlain by 20 cm of the peat-mineral mixture (Fig. 1b). The study area on the north slope of the dump was designed with a relatively uniform 5:1 incline (Fig. 1c). The toe of the hillslope is separated from a dirt road by a shallow swale constructed in glacial till. After capping the overburden, a mix of aspen and white spruce were planted on the slopes and plateau of the dump.

The dump was instrumented as part of a larger ecohydrological study to investigate the long-term evolution of the hydrological system and evaluate the success of the reclamation ecosystem. The covers were designed to provide sufficient available water-holding capacity and nutrients to support final revegetation targets (Huang et al. 2015a) and were not designed to limit pyrite oxidation. The covers were instrumented with climate monitoring stations; soil monitoring stations to measure water content, matric potential, and temperature; as well as subsurface flow trenches to capture interflow from the cover/shale interface and a set of weirs in the swale (Huang et al. 2015a; Kelln et al. 2007).

The soil water dynamics of the covers and shallow overburden are largely determined by the yearly cycle of recharge by snow melt infiltration and depletion by root water extraction. The covers freeze completely during winter (Meiers et al. 2011). When the snow pack melts, it either runs off or infiltrates into air-filled macropores

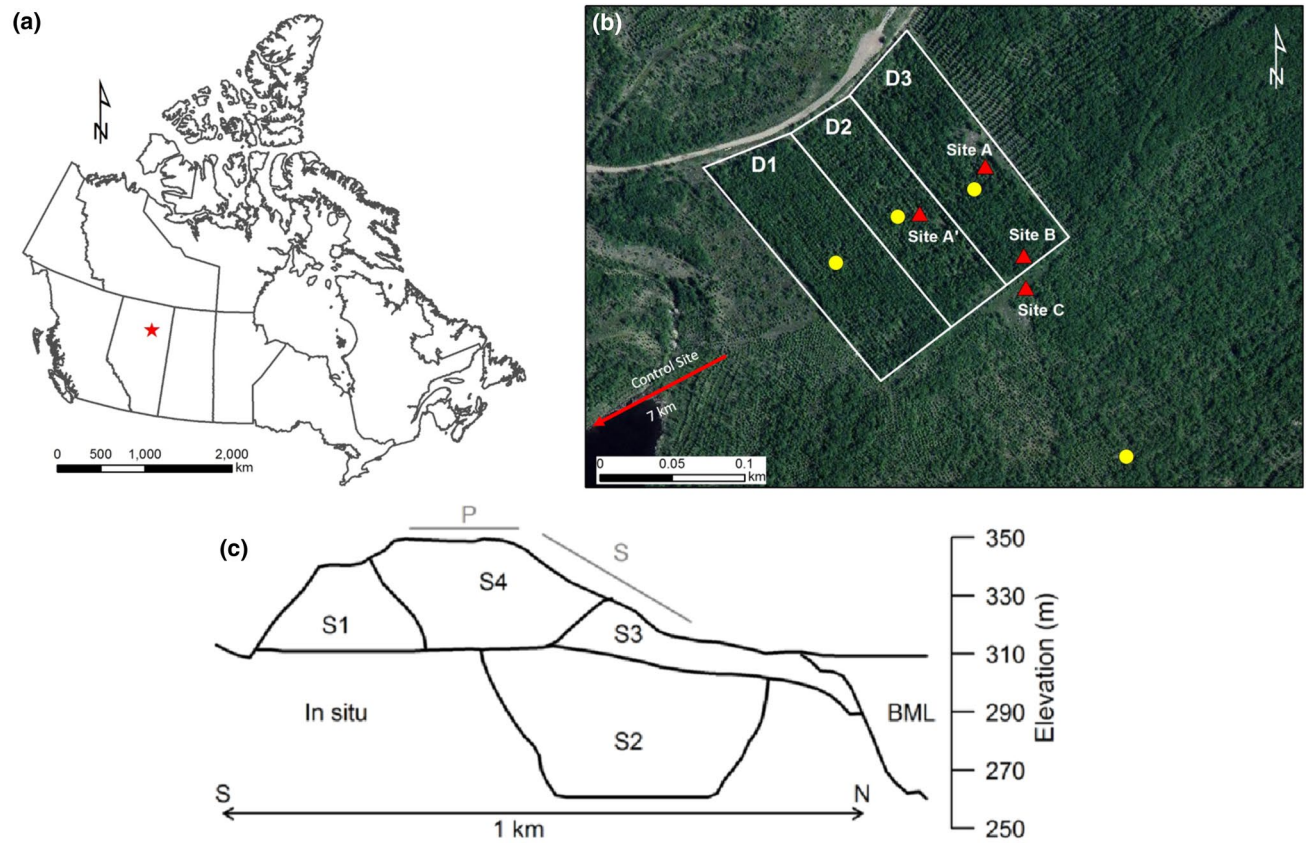

Fig. 1 **a** Site location in Canada. **b** Location of sites in the constructed watersheds on the north slope of South Bison Hill. The *red triangles* indicate the location of gas measurements and the *yellow circles* the permanent soil monitoring stations. The depths of the soil reclamation covers are from *left to right*: 0.55 m (D1), 0.35 m (D2), 1.0 m (D3). The undisturbed control site is located 7 km to the southwest of cover D1. **c** South–North cross-section of the dump (Chapman 2008). S1–S4 represent different dump phases of the overburden shale. S1: 1980–1982; S2: 1986–1990; S3: 1992–1994; S4: 1995–1996. *BML* Base Mine Lake. The *grey line* labelled "*P*" indicates the extent of the plateau, the *grey line* labelled "*S*" indicates the slope along which the constructed watersheds D1, D2, D3 are located

(Kelln et al. 2007). Subsurface flow is generated along the soil-overburden interface over the lower half of the hillslope following ground thaw (Kelln et al. 2007). During the growing season, the vegetation extracts water from the entire cover depth. Huang et al. (2015a) demonstrated that in covers less than 75 cm thick, limitations in water storage capacity can restrict transpiration during drier growing seasons. An analysis of pore water salt concentrations 3 years after placement found that salts were transported into the covers via diffusion (Kessler et al. 2010). While the diffusion profiles were similar between cover thickness and slope position, a follow-up study performed 10 years after placement showed that downward net percolation can offset the upward diffusion of salts (Huang et al. 2015b). The amount of net percolation varied with topography; percolation rates on the plateau (42–76 mm year^{-1}) were greater than on the slopes (8–34 mm year^{-1}) (Huang et al. 2015b).

Methods

Four locations within the SBH dump were sampled for chemical analysis and monitored for pore-gas concentrations (Fig. 1b). This included a mid-slope location on the D2 (0.35 m cover) watershed (site A′) and mid- and upper slope locations on the D3 (1.0 m soil cover) watershed (sites A and B), as well as one on the 1.2 m soil cover plateau (site C). A control site was selected in an undisturbed forested area 7 km southwest of the dump.

Solids Chemistry

Core samples were collected between Feb 2001 and Aug 2002 at each site using a split-spoon sampler (Table 2). The samples were split and placed in Ziploc bags. Preliminary chemical analyses of the 2001 samples indicated high concentrations of soluble sulphur at all depths indicating that oxidation likely occurred during storage of the samples.

Table 1 Geotechnical and soil hydraulic parameters of cover and shale overburden materials

Property	Peat-mineral mix	Glacial	Shale
Grain size distribution[a]			
Gravel (%)	2	2	0.5
Sand (%)	38	38	14.5
Silt and Clay (%)	60	60	85
Specific gravity[b]	2.62	2.61	2.73
Average dry bulk density (SD)[b] (g cm^{-3})	0.92 (0.31)	1.28 (0.21)	1.47 (0.20)
Atterberg limits[b]			
Plastic limit (%)	n/a	20.3	27.4
Liquid limit (%)	n/a	n/a	44.4
Porosity[c] (%)	0.56–0.59	0.44–0.55	0.44–0.57
Field saturated hydraulic conductivity (SD)[a] (m s^{-1})	7.0×10^{-5} (0.5×10^{-7})	0.4×10^{-5} (0.68×10^{-7})	0.3×10^{-7} (0.78×10^{-7})
pH[d]	5.9	7.7	7.5
EC[d] (dS m^{-1})	0.5	0.8	8.2
SAR[d] (−)	1.0	2.0	20.6

[a]Meiers et al. 2011: ASTM D422-63 method (ASTM 1996)

[b]Boese 2003: 32 samples analyzed in summer of 2000

[c]Lower value determined with optimizing of hydrological model (Huang et al. 2015b). Higher values calculated from dry density measurements (Boese 2003)

[d]Measured in saturated paste extracts (Kessler et al. 2010)

Table 2 Soil sampling details

Site	Date	# samples	Storage	Analyses
Site A	June 2001	n = 8	Aerobic	Total S, TIC, TOC, d13 of soil carbon
Site A′	June 2001	n = 12	Aerobic	Total S, TIC, TOC, d13 of soil carbon
Site B	June 2001	n = 7	Aerobic	Total S, TIC, TOC, d13 of soil carbon
Site C	Feb 2001	n = 13	Aerobic	Total S, SO_4^{2-}, TIC, TOC, d13 of soil carbon
Site C	Aug 2002	n = 30	Anaerobic	Total S, pH, EC, major ions/soluble salts Na^+, Ca^{2+}, Mg^{2+}, K^+, SO_4^{2-}, Cl^-, exchangeable cations, cation exchange capacity

To quantify the in situ soil chemistry, samples collected the following year (2002) were immediately placed in a portable anaerobic chamber (Difco Laboratories, Detroit, USA) and flushed with nitrogen to minimize oxidation. Anaerobic reaction packets were placed in each container to remove any O_2 present after flushing. The samples were then freeze-dried and ground under a nitrogen head space using a centrifuge soil grinder fitted with a 1.0 mm screen (Retsch GmbH, Haan, Germany). The samples were transferred to an anaerobic chamber (Coy Labs, Grass Lake, USA) for storage and saturated paste preparation.

The soluble salts were measured from saturated paste extracts of the soil samples (Rhoades 1982). The saturated paste extracts were prepared by mixing 100 g of each soil sample with deionized water to create a saturated paste that was then sealed in a container and allowed to equilibrate for 12 h. Leachates from the samples were filtered (0.45 µm Whatman Nuclepore filters) and diluted 100 times before analysis. One-half of each sample was acidified with a single drop of concentrated HNO_3 and analyzed for Na^+, Ca^{2+}, Mg^{2+}, and K^+ using a Dionex 2000 ion chromatograph (Thermo Scientific, Sunnyvale, USA). The non-acidified half was analyzed for pH, EC, and SO_4^{2-}, and Cl^- using the same ion chromatograph. The chemistry of the saturated paste extracts was interpreted using the equilibrium geochemical speciation program PHREEQC Interactive (Version 3.3.3; USGS 2016). All of the samples were found to be undersaturated with respect to gypsum, confirming that all of the readily soluble sulphur salts had dissolved during extract preparation.

Total S concentrations of the soil samples were measured with a LECO CNS-2000 elemental analyzer (Leco Corporation, Saint Joseph, USA). Total inorganic and total organic carbon contents of the soil samples were measured

with the LECO CR-12 carbonator carbon system (Leco Corporation, Saint Joseph, USA). The furnace temperature was set at 1100 °C for total carbon (TC) combustion and 840 °C for total organic carbon (TOC) combustion. Concentrations of total inorganic carbon (TIC) were calculated by subtracting TOC from TC concentrations. Stable carbon isotopes ($\delta^{13}C$) of TOC in solid samples were measured with a Tracer/20 mass spectrometer coupled to an ANCA g/s/l sample preparation unit (Sercon Limited, Crewe, UK). For the $\delta^{13}C$ analysis of TIC, samples were dissolved using acid-digestion to convert all of the TIC to CO_2. Samples were soaked in an excess of 3 M HCl at room temperature overnight and then rinsed with deionized water through a 45 µm filter under vacuum to remove all chloride from the samples. The samples were then dried and weighed in tin cups for mass spectrometer analysis.

The acid-generating potential of the shale overburden was quantified using an acid-base accounting (ABA) method (Morin 1990) to calculate the net neutralization potential (NNP) and the neutralization potential ratio (NPR) of the dump materials:

$$NNP = AP - NP, \quad (1)$$

$$NPR = NP/AP, \quad (2)$$

where AP is the acid generation potential (kg $CaCO_3$/tonne (t) of soil) and NP is the neutralization potential (kg $CaCO_3$/t of soil). AP was calculated from the reduced S concentrations in the soil samples, expressed as weight percentages. Assuming that all of the reduced S in the soil is available to contribute to acidification, this concentration of reduced S can be converted to kg $CaCO_3$, with the standard equations for pyrite oxidation and a conversion factor of 31.25. We assumed that all inorganic carbon (TIC) was available for acid neutralization and converted the TIC of the soil samples to kg of $CaCO_3$, with a conversion factor of 8.34.

Soil Gas Probe Installation

Total of 35 gas probes were installed in four profiles at SBH (Fig. 1b) and in one profile at the undisturbed forested site. The sites were chosen to represent different slope positions (site A vs. site B), cover thicknesses (site A vs. site A′), and conditions on the plateau (site C). At site A (midslope, 1.0 m cover), 6 gas probes were installed between the soil surface and a depth of 4.05 m; at site A′, 7 gas probes were installed between the soil surface and 1.90 m depth; at site B, 7 gas probes were installed between the soil surface and 4.45 m depth; at site C, 12 gas probes were installed between the soil surface and 25 m depth; at the control site, 3 gas probes were installed between the soil surface and 2.5 m depth.

The probes were constructed of 6.4 mm O.D. high-density polyethylene (PE) tubing with screened filters fitted on the down-hole end. The screened filters were constructed using chain-saw oil filters pushed into the tube end and covered with window screen. Holes less than 5 m deep (sites A, A′, B, and control) were hand-augered using a 50 mm diameter auger head. Each hole was filled with 5 cm of coarse sand (clean drilling sand) onto which the screened end of the probe was placed. The hole was then backfilled with another 5 cm of sand, followed by bentonite pellets to the surface. The 25 m deep hole on the plateau (site C) was augered with a truck-mounted auger drill rig (Layne Christenson Canada Ltd.) using a 100 mm diameter auger stem (200 mm outer diameter). Sand was poured in the open hole below and above each sensor with 1 m thick bentonite plugs between each pair of probes. Above ground, the PE tubing from each hole was fitted with plastic three-way valves and placed in a PVC pipe for protection.

Pore Gas Chemistry

Samples were taken from the gas-probe installations to measure pore gas concentrations of O_2, CO_2, and CH_4. The gas probes were operational from Nov 2000 (sites A, B, control) or June 2001 (site A′, C) through Oct 2003. Samples were collected from each probe monthly (2001–2002) or every other month (2003), excluding the winter season. It took approximately 6 months after installation for the probes to equilibrate with the overburden pore gas. Therefore, only data obtained after the 2001–2002 winter were interpreted in this study.

Pore gas concentrations of O_2 and CO_2 in the pore gas were measured in the field with a portable gas analyzer (GasTech Australia, Wangara, Australia) while in the second half of the sampling period, pore gas concentrations of O_2, CO_2, CH_4, and N_2 were measured with an M200 portable micro gas chromatograph (Agilent Technologies Inc., Santa Clara, USA). The GasTech analyzer was calibrated in the lab with natural air (O_2 sensor) and a gas standard (CO_2 sensor) before deployment in the field. The performance of this analyzer was checked before and after every sampling period using a gas standard containing 11.6% CO_2 (±5% of concentration) and 3.05% O_2 (±5% of concentration). Stagnant gas in the tubing of each gas probe was purged using a 50 mL plastic syringe prior to analysis.

The Agilent GC was calibrated in the lab before deployment in the field with standards of air (20.9% O_2, 78.1% N_2), and two ultra-high purity gas mixtures (UHP 1: 11.6% CO_2, 3.05% O_2, 85.35% N_2; UHP 2: 0.52% CH_4, 1.58% CO_2, 10% O_2, 88.42% N_2). Each gas port was purged using a 140 mL syringe and the final sample immediately injected into the GC for analysis. Additional gas samples were collected from the probes after each in situ pore gas analysis.

Gas samples were collected in 250 mL evacuated glass serum bottles, crimp sealed with a butyl blue septum and transported to Saskatoon for further analysis. Pore gas samples were analyzed for $\delta^{13}C_{CO2}$ with a Micromass Optima isotope ratio mass spectrometer (Waters Corporation, Milford, USA). Between Feb 2001 and Oct 2002 (when field measurements were made with the GasTech analyzer), the bottled samples were also analyzed with a Carle Special Series S311 gas chromatograph (Chandler Engineering, Broken Arrow, USA) for their concentrations of O_2, CO_2, CH_4, and N_2.

Soil Water Content and Soil Temperature

The gravimetric water content of soil samples taken from different depths during installation of the gas probes were measured in the laboratory. The volumetric water content (VWC) of these samples was then calculated using measured bulk density values for the various materials in the dump (Boese 2003). At sites A and A′, shallow access tubes were installed near the gas probe nest. Neutron counts were measured using a 503 DR Hydroprobe (CPN Inc., Concorde, USA) from Sept. 2001 through Aug. 2003. At site C, three shallow (<1.6 m) access tubes for a Diviner 2000 volumetric soil moisture profiler (Sentek Sensor Technologies, Stepney, Australia) were installed within 3 m of the gas probe nest. VWC in these profiles was obtained one to four times per month from June to Nov 2002 and from May to Aug 2003. In addition, a 20 m deep neutron access tube was installed in Aug 2002 on the plateau, 5 m from the gas probe nest. Neutron counts were measured using a 503 DR Hydroprobe (CPN Inc., Concorde, USA) from Oct 2002 through Aug 2003. Soil temperatures were measured in this access tube with a 20 m long thermistor string from May 2002 through June 2003. Additional VWC and soil temperature data was available from the soil water content and temperature monitoring stations installed as part of the larger hydrology study (Huang et al. 2015a; Kelln et al. 2007). These stations have been operational from June 1999 to present and report data twice per day. Soil temperature data from these stations were used to construct the temperature profiles of sites A and A′ on the gas sampling dates.

Quantifying Salt Release Rates and Weathering Depth

Three different methods were used to estimate the rate of SO_4^{2-} production in the field as well as the rate of propagation of the weathering front with depth as a result of oxygen ingress and consumption. In Method 1, the average SO_4^{2-} production rate was calculated based on the measurements of solid chemistry correlated to the depths of O_2 ingress observed in the field. The maximum amount of S that could be oxidized was calculated from the difference in reduced S concentrations in the soil samples in the upper, fully oxidized shale and the deeper, non-oxidized shale. It was assumed that this was all due to pyrite oxidation. It was also assumed that the initial reduced S content (prior to oxidation) was the same across the entire overburden deposit.

Method 2 calculated the SO_4^{2-} production rate from rates of oxygen diffusion into the shale. Assuming that O_2 gradients were fairly constant (quasi-steady state) and that all of the O_2 was used to oxidize reduced S, the mass of SO_4^{2-}can be calculated based on the stoichiometric relationships of pyrite oxidation, ignoring the oxidation of Fe^{2+} to Fe^{3+} and subsequent pyrite oxidation. The average O_2 mass flux into the shale overburden was calculated using the observed O_2 gradients and Fick's First Law (Eq. 5):

$$J = -\theta_{eq} D^* {}^{\partial C}/_{\partial x} = -D_e {}^{\partial C}/_{\partial z}, \tag{3}$$

where J is the molar flux of a gaseous species (M m^2 day^{-1}), θ_{eq} is the equivalent (diffusion) porosity of the porous medium (m^3 m^{-3}), D^* and D_e are the bulk and effective diffusion coefficients of O_2, respectively (m^2 day^{-1}) and ${}^{\partial C}/_{\partial z}$ is the concentration gradient with depth (M m^{-3} m^{-1}). The equivalent porosity was calculated from the air-filled and water-filled porosity θ_a and θ_w (m^3 m^{-3}), and Henry's dimensionless equilibrium constant, H, according to:

$$\theta_e = \theta_a + H\theta_w. \tag{4}$$

The value of D_e was estimated using the methods of Mbonimpa et al. (2003), which was adapted from Millington and Quirk (1961):

$$D_e = \frac{1}{n^2}\left(D_a^0 \theta_a^{p_a} + H D_w^0 \theta_w^{p_w}\right), \tag{5}$$

where n is the porosity of the medium (m^3 m^{-3}), D_a^0 and D_w^0 are the free oxygen diffusion coefficients in air and water respectively (m^2 s^{-1}), and p_a and p_w are tortuosity exponents for air and water (−) related to the basic properties of the porous medium. While methods exist to determine p_a and p_w from θ_a and θ_w, we follow Mbonimpa et al. (2003) in assuming that $p_a = p_w = 3.3$. D_a^0, D_w^0, and H are temperature dependent, so the values used in the flux calculations were based on average soil temperature (Table 3). From Eq. 5, it follows that D_e decreases strongly with increasing saturation of the pore space, with a distinct breakpoint around 80–85% saturation (Aachib et al. 2004; Mbonimpa et al. 2003).

Method 3 calculated the rate of SO_4^{2-} production with a transient analytical equation for transient gas diffusion. We assumed that the O_2 concentrations at placement were atmospheric across the cover and zero within the unoxidized shale. Following placement, near-atmospheric conditions remain at the shale surface due to the relatively higher oxygen diffusion

Table 3 Parameter values and ranges for calculations of O_2 flux and SO_4^{2-} production rates

Parameter	Min	Mean	Max	Methods using parameters
Shale bulk density (kg m^{-3})	1270	1470	1670	1, 2, 3
Reduced S content shale at placement (g S kg^{-1})	4.63	6.43	8.23	1, 2, 3
Reduced S content shale after 6 years (g S kg^{-1})	2.8	4.2	5.6	1
Depth of oxidized zone (m)	0.55	0.85	1.1	1, 2
O_2 concentration gradient (M m^{-3} m^{-1})	4.4	8.9	13.8	2
Soil temperature (°C)		8		2, 3
Porosity[a] (–)	0.44		0.57	2, 3
VWC[b] (–)	0.22	0.24	0.28	2, 3

[a]Calculations showed that 0.57 porosity was very unrealistic, considering the average VWC. We used only 0.44 porosity for calculations

[b]Volumetric water content (VWC) range (min–max) was based on variability in the shale of site C (min) and A′ (max). The average value was determined from all VWC observations in the shale of sites A, A′, and C

within the cover relative to the shale. Under these conditions, the rate at which the oxidation front advances is controlled by the coefficient of oxygen diffusion in the shale and the mass of oxidizable S within the shale. This form of conceptual model was originally developed Hendry et al. (1986) to explain the depth of weathering within glacial till in southern Alberta. This analytical solution is based on the assumption that oxygen concentrations would decrease linearly from the atmospheric boundary to zero at the depth of oxygen consumption. Under these conditions, the instantaneous oxygen mass flux (J) can be related to the mass of oxygen that will be consumed per unit soil volume (m; with units of M m^{-3}), based on the following relationship:

$$Jdt = mdz, \tag{6}$$

where t is time (day) and z (m) is depth. Substituting the gas flux J in this equation leads to:

$$-D_e \frac{\Delta C}{z} dt = mdz, \tag{7}$$

which can be solved analytically as follows:

$$z(t) = \sqrt{\frac{2D_e t}{m}} \tag{8}$$

Equation 8 was solved for a range of parameters based on observed ranges of θ, reduced S content, porosity, and soil temperature (Table 3).

Results and Discussion

Solid Chemistry

The solid and soluble chemistry in the deep overburden profile (site C, plateau) is presented in Fig. 2. The average total S concentrations of the profile in 2001 and 2002 were statistically the same, with means of $7.7 \pm 2.$ and 6.8 ± 2.3 g kg^{-1}, respectively (Student's t test at $p < 0.05$). The average soluble S concentrations in the profile were determined on cores collected in 2001 and 2002 from saturated paste extracts, but only the 2002 samples were stored and handled under anaerobic conditions and therefore were considered representative of in situ conditions. On average, the profile contained 0.37 ± 0.38 g kg^{-1} of soluble S, suggesting that 95% of the total S in the profile (6.43 ± 1.8 g kg^{-1}) was present in a reduced form. The decrease in pH caused by pyrite oxidation is buffered by the dissolution of carbonates, releasing Mg^{2+} and Ca^{2+}. Because these cations preferentially adsorb to clay particles, additional Na^+ is released into the pore water. Indeed, Na^+ was the most abundant cation in the deep profile, with values comparable to reported ranges for unsaturated shale in northern Alberta (Miller et al. 1993). By comparison, K^+, Mg^{2+}, and Ca^{2+} from saturated paste extracts displayed similar dynamics throughout the profile, but at concentrations 10–100 times lower than Na^+ (Fig. 2b). The elevated concentrations of soluble S, Na^+, K^+, Mg^{2+}, and Ca^{2+} at a depth of 1.4 m (just below the cover/shale interface) indicated oxidation at this position in the profile. The formation of a saturated paste dissolves readily soluble minerals and causes ion exchange. As such, the actual pore water at depth would have different proportions of cations than those measured in the saturated paste extracts. For example, the concentration of dissolved Ca^{2+} released by carbonate dissolution is limited by gypsum ($CaSO_4^2$) saturation and some of the SO_4^{2-} created by oxidation can be stored in the profile as gypsum. All but one of the saturated paste solutions were found to be undersaturated with respect to gypsum, indicating that all stored gypsum had been dissolved during testing (results not presented).

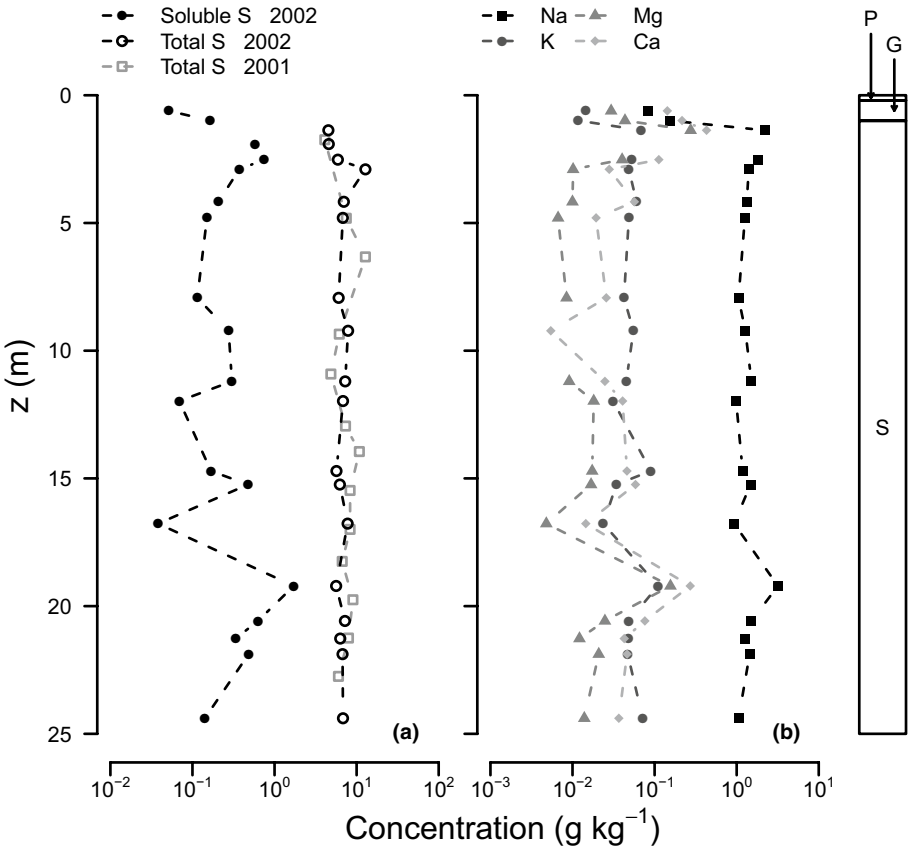

Fig. 2 Soil chemistry in the deep profile at location C (plateau): **a** total and soluble sulphur (g S kg^{-1} soil) and **b** soluble ion concentrations of saturated paste extracts as a function of depth below the soil surface. The *bar on the right of the graphs* indicates the distribution of peat-mineral mix (P), glacial soil (G), and shale overburden (S) in the profile

The total S values were consistent with reported values for undisturbed Cretaceous marine shale in North and South Dakota ,which ranged from 1.0 to 13.6 g kg^{-1} (Gautier 1986) and at the lower end of those found in these deposits in central Saskatchewan, which ranged from 10.4 to 13.3 g kg^{-1} (Nichol et al. 2016). The soluble S values in the dump profile were slightly less than the reported values for undisturbed shale in southern Saskatchewan, which ranged from 0.13 to 4.8 g kg^{-1} with an average soluble S concentration of 1.3 g kg^{-1} (Mermut and Arshad 1987). In undisturbed shale deposits, concentrations of oxidation products exhibit the greatest variability close to the land surface (Mermut and Arshad 1987). In the dump profile, concentration variability was observed not only at the surface, but also at depths of approximately 15–20 m (Fig. 2). The combination of elevated soluble S, Na^{+}, Ca^{2+}, and Mg^{2+} concentrations and the average total S concentration suggests oxidation may have occurred along a previous lift surface prior to continued construction of the dump. The construction history of the dump is consistent with this observation as there were periods during which the overburden was exposed to the atmosphere before being covered by a new lift (Chapman 2008).

Assuming all of the reduced S in the profile (Fig. 2a) was available for oxidation to SO_4^{2-} and estimating the kg $CaCO_3$ per tonne of soil from the TIC concentrations in the same profile (as addressed below), an average net neutralizing potential (NNP) of -6.3 ± 1.8 kg $CaCO_3$/t soil was determined for the shale soil samples. The negative NNP reflects the limited potential for the creation of acid drainage although predictions of acid generating potential are difficult for NNP values between −20 and +20 kg $CaCO_3$/t soil (Morin 1990; Steffen Robertson and Kristen Inc. 1989). However, when combined with a neutralizing potential ratio (NPR) value of 59.9 ± 120, the AMD leaching potential from this overburden dump is considered to be low (Price et al. 1997).

The total S concentrations in the shale were also determined mid-slope on the hillslopes, under the 1 and 0.35 m soil cover (site A and site A′, respectively). The average values of 4.40 ± 1.8 and 5.50 ± 1.5 g kg^{-1} total S at these sites was lower than, but not statistically different from, the concentrations in the deep profile (Student's *t* test at $p < 0.05$). The samples from the glacial layer of the soil covers at these locations featured higher total S concentrations than natural weathered glacial till deposits (1.30 ± 1.2 g kg^{-1} S), compared to 0–1 g kg^{-1} in southern Saskatchewan and Alberta (van Stempvoort et al. 1994). These elevated S concentrations may be attributed to diffusion of soluble S from the overburden into the covers

(Hilderman 2011; Kessler et al. 2010). Unfortunately, soluble S concentrations were not determined on these samples.

Pore Gas Chemistry

Concentration Profiles

Consistent with observations from other weathered till soils (Keller and Bacon 1998), the concentrations of O_2 and CO_2 at the control site were constant to a depth of 2.5 m over the measurement period (Fig. 3g), averaging $19.9 \pm 1.0\%$ O_2 (interquartile range IQR 1.5) and $0.74 \pm 0.64\%$ CO_2 (IQR 1.26). No CH_4 was detected at the control site. The pore gas concentrations within the overburden differed markedly from those of the natural profile. Sharp decreases in the O_2 concentrations and corresponding increases in the CO_2 concentrations were observed between 1.0 and 1.7 m below the soil surface at the three hillslope sites (Fig. 3a, d, h). Hillslope position (sites A vs. B) and soil cover thickness (sites A vs. A′) did not appear to influence the depth

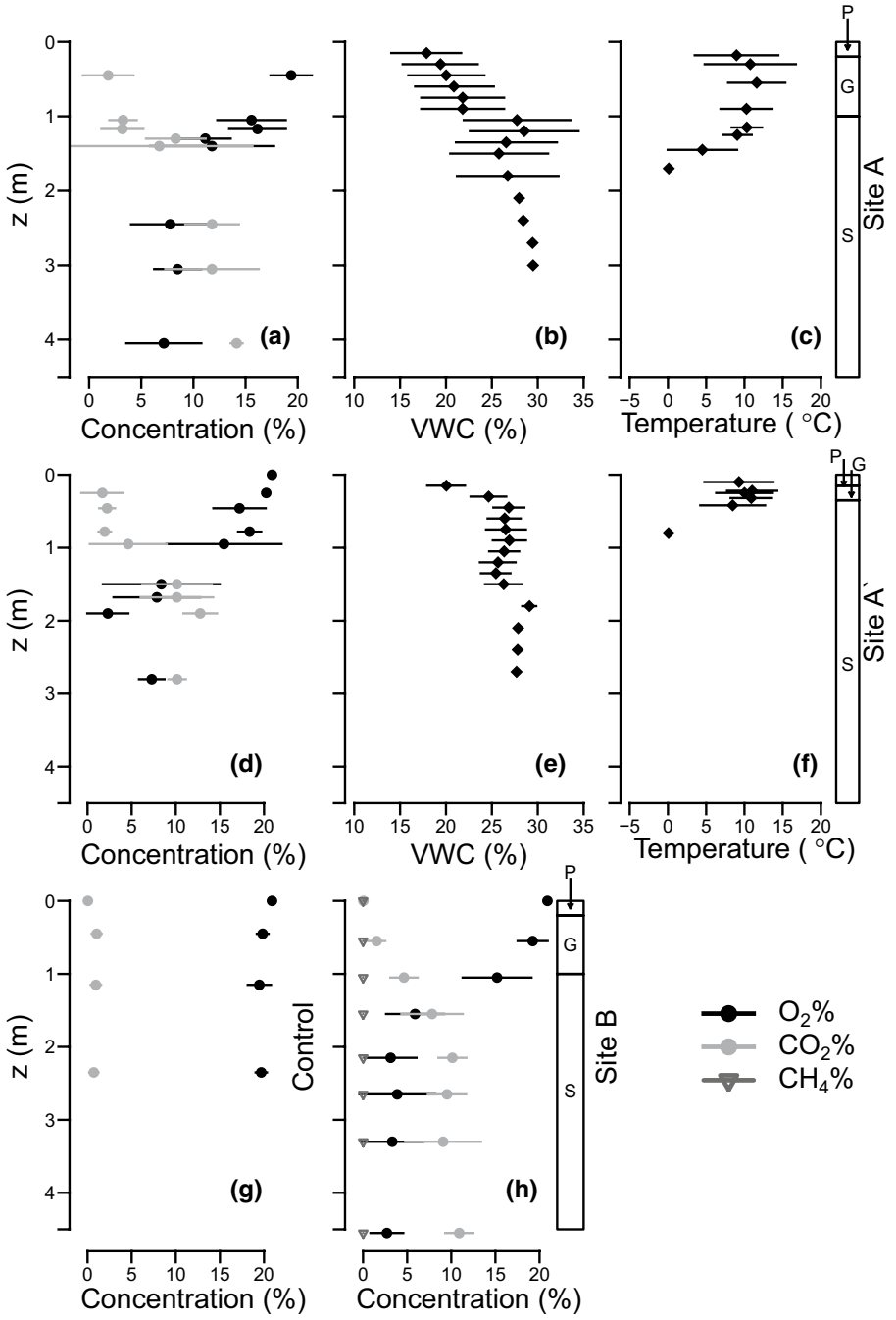

Fig. 3 Pore gas concentrations, volumetric soil water content (VWC), and soil temperature collected from June 2001 to Oct 2003. The *bars* on the right of the pore gas concentration panels show the distribution of peat-mineral mix (P), glacial soil (G), and shale overburden (S) in the profiles. The *points* indicate mean values, the *whiskers* extend to ±1 SD. At the control site and upslope site B, VWC and soil temperature were not available, therefore only pore gas concentrations are shown for these locations

of the gas concentration transition zones relative to the ground surface. Consequently, deeper ingress of O_2 into the shale overburden occurred at site A′ (1.4 m) than at sites A and B (0.75 and 0.90 m, respectively), as a result of the differences in cover thickness at these sites. O_2 concentration fluctuations (quantified by width of horizontal lines through the symbols in Fig. 3) were greater at the 0.35 m soil cover site A′ than at the 1 m soil cover sites A and B. Under the 0.35 m cover (site A′) however, elevated O_2 levels continued unabated within the upper meter of overburden. Plotted as a function of depth below the soil surface, the concentration profile was consistent with those from the other sites. Below 1.7 m, O_2 concentrations decreased to 3.4% (site B), 6.9% (site A′), and 8.8% (site A). In contrast, CO_2 concentrations below 1.5 m fluctuated most at site A. Average CO_2 concentrations below 1.7 m depth were 9.9% (site B), 11.0% (site A′), and 12.6% (site A). The gas concentration profiles at site C exhibited a sharp decrease in O_2 and increase in CO_2 near the ground surface, similar to that of the other sites (Fig. 4). The measurement resolution in the deep profile (site C) was not sufficient to locate the steepest part of the weathering front other than that it was shallower than 3.5 m (Fig. 4). O_2 concentrations decreased to 0.5% below 5 m, while CO_2 concentrations fluctuated around 4% from 5 to 20 m of depth and decreased slightly below that. Methane was present in the profiles of site B and site C (Figs. 3h, 4c respectively). At site B, CH_4 was detected at depths below 1 m, reaching a steady and uniform concentration of $0.01 \pm 0.012\%$ (IQR 0.017%). At site C, greater than atmospheric CH_4 concentrations were observed in the profile at depths ≥3.5 m at an average concentration of $1.1 \pm 0.13\%$ (IQR 0.29%). CH_4 concentrations increased with depth from 5 to 15 m and varied with time. Below 15 m, CH_4 concentrations fluctuated around 1.4%. In general, the shapes of the O_2 profiles at sites A and B (Fig. 3a, h) were consistent with relatively unrestricted diffusion across the cover layer and diffusion and consumption within the upper meter of the shale. Profiles with such sharp transitions have also been observed in highly reactive coarse textured mine waste rock dumps (e.g. Gelinas et al. 1992; Lefebvre et al. 2001b; Sracek et al. 2004).

Temporal dynamics in gas concentrations would be expected as a result of progression of the weathering front into the overburden (time scale: years) and as a function of biological activity or soil moisture variability (time scale: months) (Hendry et al. 1999; Keller and Bacon 1998). Changes in the O_2 and CO_2 gradients were observed in the individual profiles (Fig. 5). The concentration gradient was greatest in May and decreased during the growing season, to increase again in late fall and the next winter. This would be consistent with a conceptual model in which higher water contents within the cover soils in the spring and fall restrict oxygen diffusion into the shale. As the water content within the covers decreases over the summer months, the oxygen gradients within the cover soils decrease, even though the oxygen diffusion rates through the covers likely increase. Such a seasonal dynamic was small in our profiles, contrary to a fine tailings sand site on the same mine property where cyclical O_2 patterns were observed to 3 m below the soil surface (Birkham et al. 2007). The

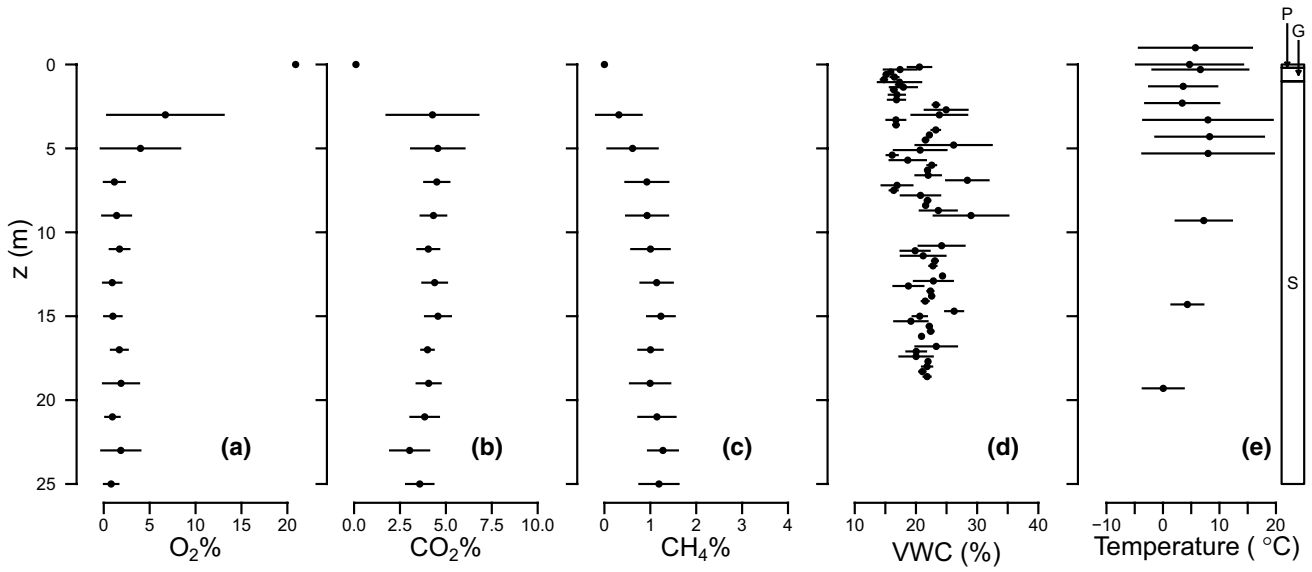

Fig. 4 Pore gas concentrations, volumetric soil water content, and soil temperature in the deep profile on plateau site C collected from June 2001 to Oct 2003. The *bar* on the right shows the distribution of peat-mineral mix (P), glacial soil (G), and shale overburden (S) in the profile. The *points* indicate mean values, the *whiskers* extend to ±1 SD

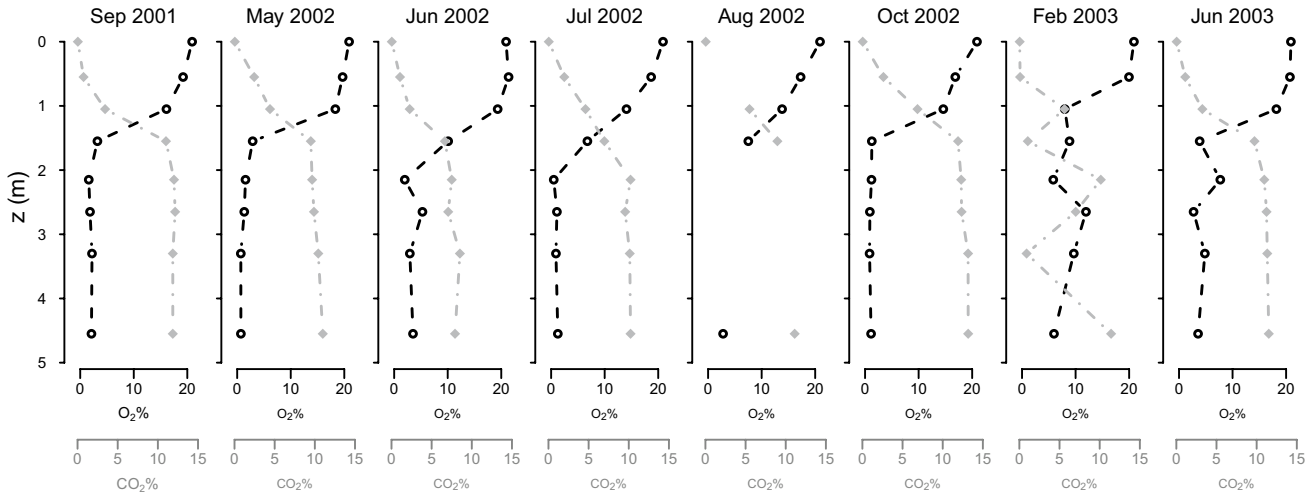

Fig. 5 Profiles of O_2 and CO_2 concentrations at site B during the entire field campaign

monitoring period was, however, too short to observe a downward migration of the weathering front based on pore gas concentrations. For example, the O_2 concentrations in Oct 2003 (last measurement of this study) were not consistently greater than those in May 2002, nor were the CO_2 concentrations in Oct 2003 consistently less than those in May 2002.

It is likely that gas transport rates would also be affected by snow on the ground and frozen soil conditions. Thick, wet snow packs can reduce O_2 ingress into the soil as well as CO_2 release to the atmosphere (Sommerfeld et al. 1996), whereas frozen soil layers enhance the trapping of pore-gas, increasing the seasonal and spatial variability of CO_2 concentrations (Winston et al. 1995). Low soil temperatures slow down oxidation reaction rates, but when a steady oxygen supply is maintained, pyrite oxidation will continue at temperatures below freezing (Elberling 2005). The maximum snow depth at the sites during the 2002–2003 winter was 27 cm (equivalent water volume of 20 mm), which is unlikely to have greatly hampered gas exchange between the soil and the atmosphere (Sommerfeld et al. 1996). The profiles of pore-gas concentration were, however, more variable during winter than summer (Fig. 5). With an average frost depth between 1.75 and 2.3 m below the surface during the 2002–2003 winter, soil frost may have affected the diffusion process.

Origin of Gases

The presence of pore-gas CH_4 in the profile can either be evidence of production at depth or of degassing and diffusion of CH_4 that was present in the shale prior to placement in the dump. Hendry et al. (2016) have documented concentrations within undisturbed Cretaceous shale pore-fluids increasing from 40 mg L^{-1} near the top of the formation to 120 mg L^{-1} at depths of 100 m in the shale. Excavation and placement of the overburden shale into unsaturated dumps would consequently be expected to result in degassing of this CH_4 and its subsequent upward diffusion. The overburden dump at our site also contains lean oil sands, which could result in CH_4 generation.

The $\delta^{13}C$ of the pore CO_2 in the profiles was determined during five sampling events (Fig. 6a, c). The effects of multiple isotopic fractionation processes during reaction and during transport by diffusion may complicate isotopic signatures in soils beyond simple mixing models (Sihota and Mayer 2012), but an initial assessment can be made. Atmospheric CO_2 has an average $\delta^{13}C$ signature of ≈−8‰, which is seen in the surface sample from site C. In soils, CO_2 is produced from organic carbon through heterotrophic microbial production/respiration of soil organic matter with an average $\delta^{13}C$ of ≈−25‰, and released via autotrophic root respiration with more depleted $\delta^{13}C_{CO2}$ values of the released pore gas CO_2 (≈−28‰ for C3 plants) (e.g. Millard et al. 2010). The organic carbon had an average $\delta^{13}C_{TOC}$ of -26.25 ± 1.3‰, ranging from −25 to −29‰. By contrast, the average $\delta^{13}C_{TIC}$ determined from soil samples of the plateau profile was -5.20 ± 9.7‰, with a range of −20 to +14‰. In the presence of biogenic ($\delta^{13}C$ −40 to −80‰) or thermogenic ($\delta^{13}C$ −20 to −40‰) CH_4, oxidation can produce pore-gas CO_2 with a similarly depleted $\delta^{13}C$ signature.

At sites A′, B, and in the upper 17 m of site C, the $\delta^{13}C_{CO2}$ values showed that inorganically produced CO_2 dominated the total gas concentration. At site A and below 17 m in the profile of site C, the signature indicated non-negligible contributions of organic carbon from respiration or methane oxidation. These fluctuations and differences

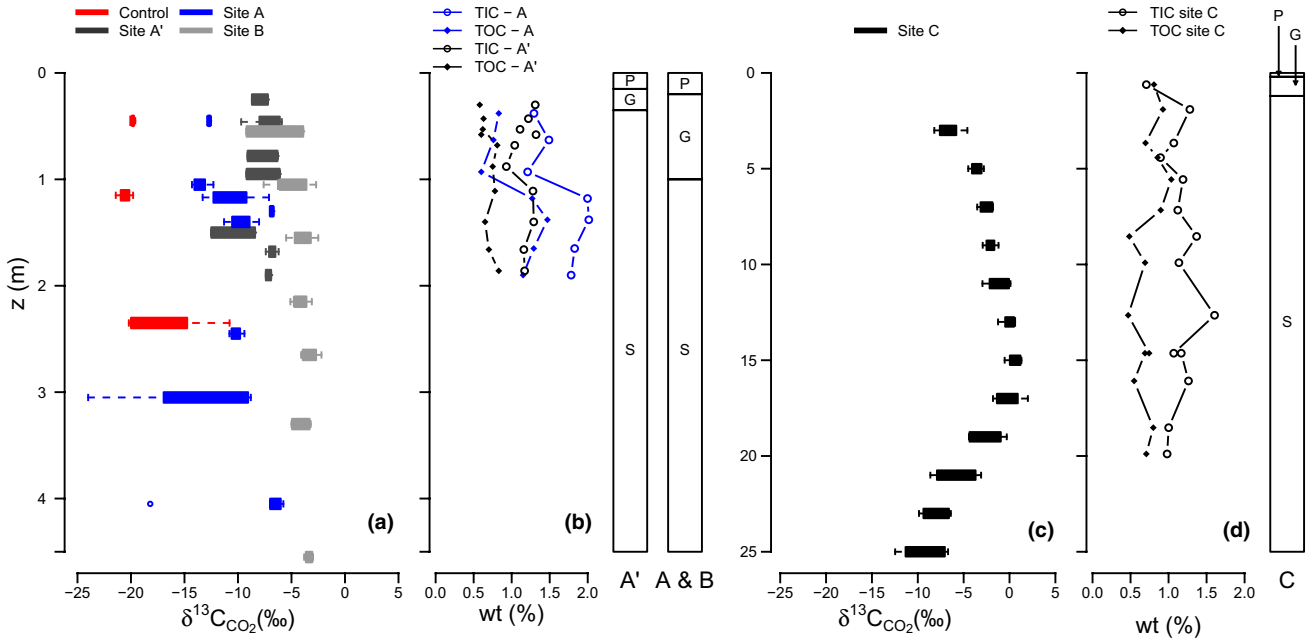

Fig. 6 The $\delta^{13}C_{CO2}$ fraction of in the pore gas CO_2: **a** shallow profiles of hillslope sites A, A′, and B and the control site; **c** deep profile of site C (plateau). For comparison, the Total Inorganic Carbon (TIC) and Total Organic Carbon (TOC) concentrations are presented in panels **b** and **d**. Data collected between June 2001 and Oct 2003. The *width of the boxes* represents the interquartile range (IQR), the *whiskers* minimum and maximum values

could not be related to variability of TIC and TOC concentrations in the profiles (Fig. 6b, d). Respiration seems unlikely at depths ≥5 m; therefore, the declining CO_2 concentrations below 17 m in the profile may indicate that some CH_4 was oxidized to CO_2 in the lower portion of the profile.

Soil Water Content and Temperature

The statistics of VWC in the profiles of sites A, A′, and C, measured during the gas sampling period, are presented in Figs. 3b, e, 4d. At sites A and A′, a clear increase in VWC can be observed at 1 m (site A) and 0.5 m and 1.7 m (site A′) from the surface. At site A, this increase corresponded to the interface between the soil cover and the shale overburden, whereas at site A′, this increase occurred at the interface and deeper into the shale. At both sites, the VWC was high and constant over the course of the observation period at depths below 2 m. At site C, the variability of VWC was large over the entire profile, though not at all depths (Fig. 4d). This site was characterized by a dry upper 3 m of cover and overburden, increased wetness to a depth of 5 m, followed by a relatively constant VWC (≈22%).

The soil temperatures in the soil covers and shallow overburden (<5 m) during the growing season fluctuated between −5 and +20 °C (Figs. 3c, f, 4e), with an average of 8.8 ± 4.7 °C. On the hillslopes, soil temperatures fluctuated with the seasonal air temperature and soil covers freeze to their full depth during the winter (long-term data not presented here, partially available in Meiers et al. 2011). The average temperature deeper in the overburden was calculated from seven thermistor measurements at site C during the summer of 2002 (Fig. 4e) and found to be 3.0 ± 4.7 °C. At such temperatures, biological oxidation rates will be reduced (Elberling 2005).

Pyrite Oxidation: Salt Release Rates and Propagation of the Weathering Front

Method 1: Solids Analysis

The simplest estimate of pyrite oxidation rate was obtained from the difference in concentrations of reduced S in the shallow and deep overburden. The O_2 concentrations in the shallow profiles suggest that oxidation had taken place to depths of 0.55–1.1 m into the overburden shale (Table 3). The solid samples in this depth range in the deep profile

had a reduced S concentration of 4.2 g kg^{-1}, whereas those in the lower part of the profile (where no oxidation had taken place) had an average concentration of 6.7 g kg^{-1} (Fig. 2). Assuming all overburden had the same initial concentration of reduced S, the average SO_4^{2-} production rate over the 6 years since dump construction was 3.4×10^{-3} g SO_4^{2-} kg^{-1} day^{-1}. This corresponds to a production rate range of 1.98 to 7.22 g SO_4^{2-} m^{-2} day^{-1} (equivalent to $3.6\times10^{-2}-1.3\times10^{-1}$ M O_2 m^{-2} day^{-1}) for the range of observed oxidation depth and dry bulk density of the shale (Table 3). The analysis is unable to estimate changes in oxidation rates with time and may under-estimate the production rates since it does not account for any SO_4^{2-} that has been removed from the shale by upward diffusion into the cover.

Method 2: Oxygen Diffusion Analysis

The second estimate of the SO_4^{2-} production rate was made by calculating the O_2 mass flux into the overburden at the time of the measurement campaign from the O_2 concentration gradient in the profiles (Fick's first law, Eq. 3) and by assuming that all of the O_2 was consumed by pyrite oxidation. Equation 3 requires measured values for the O_2 concentration gradient, as well as the volumetric water content, porosity, and soil temperatures, from which θ_e and D_e can be calculated (Eqs. 2 and 3, respectively). While the overall shape of the O_2 concentration profiles at the locations were similar Fig. 3, a range of O_2 concentration gradients from 4.4 to 13.8 M m^{-3} m^{-1} was calculated from the individual profiles (Fig. 5). VWC and soil temperature values (Table 3) were chosen from the observations during the field campaign (Figs. 3, 4). Only one average temperature value was used since depth or temporal variations in VWC tend to dominate the value of D_e. The average VWC was determined from all observations in the shale at sites A, A′, and C. The minimum and maximum values were calculated from the deeper measurements at the individual sites: the VWC at depths of 3–4 m at sites A and A′ being wetter (average 28%) than the VWC below 3 m at site C (average 22%).

Even when considering that the greatest concentration gradients occurred when air-filled porosity was lowest (i.e. in fall and spring), the resulting range of O_2 fluxes and associated SO_4^{2-} production rates were large, exceeding those estimated from the geochemistry of the solid samples, ranging from 7.4×10^{-2} to 6.6×10^{-1} M O_2 m^{-2} day^{-1} (equivalent to 4.1 to 36.3 g $SO_4^{2-}m^{-2}$ day^{-1}). For the ranges of oxidation zone thickness and reduced overburden S content (Table 3), these rates translated to an SO_4^{2-} production rate of 2.9×10^{-3} to 4.0×10^{-2} g SO_4^{2-} kg^{-1} day^{-1}, with a value of 1.4×10^{-2} g SO_4^{2-} kg^{-1} day^{-1} under average conditions. This method may overestimate actual SO_4^{2-} production rates when VWC and O_2 gradients are predominantly determined in warm, dry periods of the year.

Method 3: Analytical Model

The average values of VWC and soil temperature discussed in the previous section were also used as input to D_e in this third method (Table 3). The main assumption is that all of the O_2 diffusing into the overburden is consumed by pyrite oxidation, i.e. all reduced S present to a certain depth needs to be oxidized before the weathering front can progress downward. Following the general stoichiometry of pyrite oxidation, every mole of reduced S requires 1.75 mol O_2 to oxidize. The range of O_2 consumption per m^3 of soil was calculated from the reduced S concentration measured in the soil samples and the bulk density of the shale (Table 3). As noted before, this is a simplification of the oxidation process, because pyrite oxidation by $Fe_2(SO_4)_3$ is not considered.

The range of SO_4^{2-} production rates simulated with this model fell between those calculated from the soil samples and from the O_2 gradient at the time of the field campaign (Fig. 7a). The simulated rate of propagation of the oxidation front for average field conditions overestimated the oxidation depth, compared to the observed oxidation depths from soil sampling and gas monitoring (Fig. 7b). As in Method 2, the SO_4^{2-} production rates calculated with this procedure may overestimate actual production rates when the average VWC from the measurements is biased towards dry periods of the year.

Synthesis

The overestimation of SO_4^{2-} production and oxidation depth by the analytical solution can be explained by considering the two distinct hydrological seasons that occur on site. With the exception of Feb 2003, our sampling was performed during the growing season when the soil was not frozen and root water uptake was occurring. Saturation of the lower parts of the covers is common in May or June, after soil thaw, but rare during most other months (Huang et al. 2015a; Kelln et al. 2007), While soil freezing may leave macro-pores open all the way into the overburden, freeze up of the covers after a wet fall and snow pack development may effectively limit the oxidation process during winter. Our sampling pattern will thus have overestimated the effective porosity for diffusion. This preferential sampling would have also affected the quasi-steady state calculation of the rate of SO_4^{2-} production from the O_2 concentration gradients.

The SO_4^{2-} production rates calculated with these three methods are all at the higher end of a range of estimates obtained from optimization of hydrological models

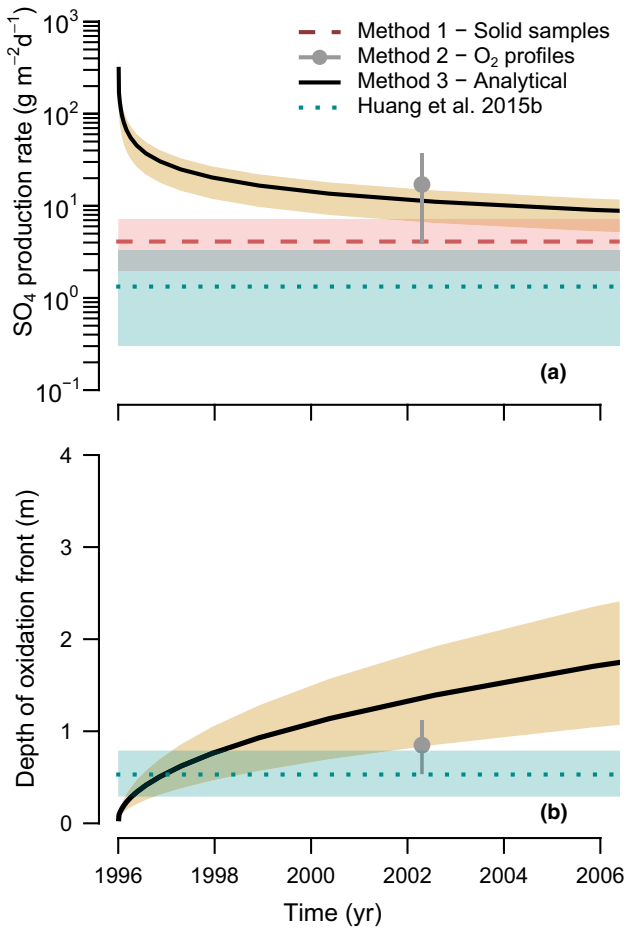

Fig. 7 **a** Sulphate production rate in the overburden dump as a function of time estimated from the solid samples, gas concentration profiles, and analytical model. The *shaded polygons* indicate the range of rates for the parameter combinations presented in Table 3. **b** Propagation of the oxidation front into the shale overburden as a function of time estimated from the gas concentration profiles and analytical model. The *shaded polygons* indicate the range of depths for the parameter combinations presented in Table 3

for the sites by Huang et al. (2015b), who found average rates of 1.89 and 0.30 g SO_4^{2-} m^{-2} day^{-1} for various locations on the 1 m cover catchment (where sites A and B were located) and a min–max range of 0.7–3.32 g SO_4^{2-} m^{-2} day^{-1} for the plateau (where site C was located). In the Huang et al. (2015b) study, oxidation depths were optimized concurrently, resulting in average depths of 0.36, 0.29, and 0.79 m, for locations close to sites A, B, and C, respectively. These depths (representing a period of 10 years after placement) were low compared to the O_2 ingress observed 6 years after placement in the current study.

From an ecohydrological perspective, shale oxidation rates should vary between sites with different cover thicknesses, such as between sites A and A′. The presence of a wetter layer would typically be expected at the glacial-shale interface due to the low saturated hydraulic conductivity (K_s) of the shale (2×10^{-9} m s^{-1}) relative to that of the glacial till in the covers (2×10^{-6} m s^{-1}; Meiers et al. 2011). This hydraulic conductivity contrast is a key control on the available water storage capacity of the cover as well as the generation of lateral subsurface flow in spring (Kelln et al. 2007, 2008, 2009). The formation of such a saturated layer is the basis used to design covers to limit oxygen ingress (Yanful et al. 1993). When the soil cover is thin (on this particular site, thinner than 0.75 m), vegetative water demand results in low seasonal VWC across the entire cover depth (Huang et al. 2015a) and sometimes extending into the upper shale surface. This allows faster O_2 diffusion rates into the overburden. Indeed, our observations show that at site A′, O_2 penetrated deeper into the shale than at site A (Fig. 3). However, the VWC profiles of site A′ suggest that the porosity and K_s of the upper shale at this site may have been compromised relative to that of site A, mostly likely due to freezing extending deeper into the shale at this location, due to the thinner cover. As a result, the VWC in the upper shale was less at site A′ than at site A, enhancing the local oxidation rate.

While hydrological processes typically vary as a function of hillslope position, we did not find differences in pore gas concentration profiles between our midslope and upslope sites (site A and B, Fig. 3). We do not have full hydrological data for site B, but it seems plausible that differences would be observed when looking at sites further downhill. After snowmelt and soil thaw, a perched saturated zone can develop in the covers, which would affect O_2 penetration. However, this zone does not extend beyond 20 m from the toe of the hillslopes (Kelln et al. 2008). Larger hydrological differences, especially in terms of net percolation, have been observed between the midslope sites and the flat plateau (Huang et al. 2015b). Unfortunately, gas sampling at the plateau (site C) was not performed at small enough intervals in the shallow soils for a detailed comparison with sites A and B.

In relatively wet soils, like those present in this dump (Figs. 3, 5), the advance of the weathering front is so slow that the increases of O_2 concentrations at depth over the period of a year were likely overshadowed by heterogeneity in the profiles and were not detectable with the techniques used in this study (Fig. 6). It is apparent from the observations and calculations (Fig. 7b) that monitoring over a period of at least 5–10 years would be required to define the advance of the oxidation front using pore-gas monitoring.

Conclusions

This study presented results of a geochemical survey and analytical investigation of the weathering processes at a shale overburden dump in the oil sands region of northern Alberta. Sulphide mineral oxidation, carbonate mineral dissolution, and ion exchange were the primary geochemical reactions occurring in the 25 m thick profile of the unsaturated, saline-sodic waste pile. The chemistry of soil samples from the unoxidized 5–25 m depth portion of the dump showed total (6.7 g total S kg^{-1} soil) and reduced S (6.51 g S kg^{-1} soil) concentrations, which were similar to those observed in natural shale deposits. Increased masses of soluble sulphur near the ground surface provided evidence of pyrite oxidation. Indications of oxidation were also observed at a depth of about 17 m and were attributed to exposure of the shale overburden to the atmosphere during dump construction. Based on acid base accounting, the overburden waste pile is not at risk for acidification.

Gas concentration profiles for locations with different cover thicknesses and slope positions were similar. At the time of the study, the depth that O_2 penetrated into the overburden was between 1.35 and 2.75 m below the soil surface and 0.55 to 1.1 m into the overburden. The $\delta^{13}C$ analysis of the CO_2-carbon confirmed the mineral origin of most of the CO_2 in the profile. At shallow depths, the CO_2 concentrations mirrored those of O_2, with increasing CO_2 with decreasing O_2. In the deep profile, CO_2 concentrations were high and O_2 was absent. Methane was present in two of the five profiles. The source of the CH_4 was not defined but was likely due to either degassing of CH_4 present in the pore-fluid of the shale prior to mining or CH_4 generation associated with the presence of hydrocarbons within the dump. Calculations based on the solid chemistry, O_2 pore gas observations, and analytical simulations yielded a range of SO_4^{2-} production rates of 4.2 to 17.1 g SO_4^{2-} m^{-2} day^{-1} 6 years after dump construction, which for the observed O_2 penetration depths, corresponds to 3.4×10^{-3} to 13.7×10^{-3} g SO_4^{2-} kg^{-1} day^{-1}. The SO_4^{2-} production rates and progression of the weathering front obtained from observations and simulations agreed reasonably well.

To better account for the observed variability, the degree of coupling and rigor used to characterize cover hydrology, gas transport, and pyrite oxidation will need to be improved. In particular, it is important to quantify the impact of seasonality and cover thickness on oxidation rates as a function of cover thickness. Such a coupling may be able to verify the hypothesis that wetness differences between thick and thin soil covers control the penetration of freeze–thaw and wetting–drying cycles, and consequently the oxidation processes, into the shale. Any further modeling efforts would also need to account for the presence of macro-pores such as cracks, which may be an exacerbating factor. These analytical efforts would need support from further observations of the gas profiles over the winter season to observe how seasonal soil moisture dynamics and the winter period (in which soil is frozen, but macropores remain air-filled) affect the variability of oxidation rates and O_2 ingress.

Acknowledgements The authors gratefully acknowledge the support of Syncrude Canada Ltd. as well as funding from the Cameco-Natural Sciences and Engineering Research Council of Canada Industrial Research Chair (MJH; Grant 184573) and a Syncrude-Natural Sciences and Engineering Research Council of Canada Industrial Chair (SLB; Grant 428588). We thank Stephanie Villeneuve for designing Fig. 1.

References

Aachib M, Mbonimpa M, Aubertin M (2004) Measurement and prediction of the oxygen diffusion coefficient in unsaturated media, with applications to soil covers. Water Air Soil Poll 156(1):163–193

Amos RT, Blowes DW, Bailey BL, Sego DC, Smith L, Ritchie AIM (2015) Waste-rock hydrogeology and geochemistry. Appl Geochem 57:140–156

ASTM (1996) Standard test method for particle size analysis of soils. D422-63; Annual Book of ASTM Standards, Vol 4.08, Philadelphia, pp 10–16

Birkham TK, Hendry MJ, Wassenaar LI, Mendoza CA (2007) A transient model of vadose zone reaction rates using oxygen isotopes and carbon dioxide. Vadose Zone J 6(1):67–76

Boese CD (2003) The Design and Installation of a Field Instrumentation Program for the Evaluation of Soil-Atmosphere Water Fluxes in a Vegetated Cover over Saline/sodic Shale Overburden. MSc Diss, University of Saskatchewan, Saskatoon

Chapman DE (2008) Hydrogeologic Characterization of a Newly Constructed Saline-Sodic Clay Overburden Hill. MSc Diss, University of Saskatchewan, Saskatoon

Elberling B (2005) Temperature and oxygen control on pyrite oxidation in frozen mine tailings. Cold Reg Sci Technol 41(2):121–133

Emrich, GH, GL Merritt (1969) Effects of mine drainage on groundwater. Groundwater 7(3):27–32

Gautier DL (1986) Cretaceous shales from the western interior of North America: sulphur/carbon ratios and sulphur-isotope composition. Geology 14(3):225

Gelinas P, Lefebvre R, Choquette M (1992) Monitoring of acid mine drainage in a waste rock dump. In: Singhal R, Mehrotra AK, Fytas K, Collins JL (eds), Environmental issues and waste management in energy and minerals production. Balkema, Rotterdam, pp 742–756

Government of Alberta (2016) http://www.alberta.energy.ca. Accessed 12 June 2016

Haug KM, Greene P, Mei S (2014) Geological Characterization of the Lower Clearwater Shale in the Athabasca Oil Sands Area, Townships 87–99, Ranges 1–13, West of the Fourth Meridian. AER/AGS Open File Report 2014-04. Alberta Energy Regulator/Alberta Geological Survey, Edmonton

Hendry MJ, Cherry JA, Wallick EI (1986) Origin and distribution of sulphate in a fractured till in southern Alberta, Canada. Water Resour Res 22(1):45–61

Hendry MJ, Mendoza CA, Kirkland RA, Lawrence JR (1999) Quantification of transient CO_2 production in a sandy unsaturated zone. Water Resour Res 35(7):2189–2198

Hendry MJ, Barbour SL, Schmeling E, Mundle SO, Huang M (2016) Fate and transport of dissolved methane and ethane in Cretaceous shales of the Williston Basin, Canada. Water Resour Res 52:6440–6450

Hilderman, JN (2011) Net percolation as a function of topographic variation in a reclamation cover over a saline-sodic overburden dump. MSc Diss, University of Saskatchewan, Saskatoon

Huang M, Barbour SL, Carey SK (2015a) The impact of reclamation cover depth on the performance of reclaimed shale overburden at an oil sands mine in northern Alberta, Canada. Hydrol Process 29(12):2840–2854

Huang M, Hilderman JN, Barbour SL (2015b) Transport of stable isotopes of water and sulphate within reclaimed oil sands saline-sodic mine overburden. J Hydrol 529:1550–1561

Keller, CK, Bacon DH (1998) Soil respiration and georespiration distinguished by transport analyses of vadose CO_2, $13CO_2$, and $14CO_2$. Global Biogeochem Cycles 12(2):361–372

Kelln CJ, Barbour SL, Qualizza CV (2007) Preferential flow in a reclamation cover: hydrological and geochemical response. J Geotech Geoenviron 133(10):1277–1289

Kelln CJ, Barbour SL, Qualizza CV (2008) Controls on the spatial distribution of soil moisture and solute transport in a sloping reclamation cover. Can Geotech J 45(3):351–366

Kelln CJ, Barbour SL, Qualizza CV (2009) Fracture-dominated subsurface flow and transport in a sloping reclamation cover. Vadose Zone J 8(1):96–107

Kessler S, Barbour SL, KCJ van Rees, Dobchuk BS (2010) Salinization of soil over saline-sodic overburden from the oil sands in Alberta. Can J Soil Sci 90(4):637–647

Lefebvre R, Hockley D, Smolensky J, Gelinas P (2001a) Multiphase transfer processes in waste rock piles producing acid mine drainage 1: conceptual model and system characterization. J Contam Hydrol 52(1–4):137–164

Lefebvre R, Hockley D, Smolensky J, Lamontagne A (2001b) Multiphase transfer processes in waste rock piles producing acid mine drainage: 2. applications of numerical simulation. J Contam Hydrol 52(1–4):165–186

Lottermoser BG (2010) Mine wastes: characterization, treatment and environmental impacts. Springer, Berlin

Mbonimpa M, Aubertin M, Aachib M, Bussière B (2003) Diffusion and consumption of oxygen in unsaturated cover materials. Can Geotech J 40(5):916–932

Meiers, GP, SL Barbour, CV Qualizza, BS Dobchuk (2011) Evolution of the hydraulic conductivity of reclamation covers over sodic/saline mining overburden. J Geotech Geoenviron 137(10):968–976

Mermut AR, Arshad MA (1987) Significance of sulphide oxidation in soil salinization in southeastern Saskatchewan, Canada. Soil Sci Soc Am J 51(1):247–251

Millard P, Midwood AJ, Hunt JE, Barbour MM, Whitehead D (2010) Quantifying the contribution of soil organic matter turnover to forest soil respiration, using natural abundance $\delta^{13}C$. Soil Biol Biochem 42(6):935–943

Miller JJ, Pawluk S, Beke GJ (1993) Soil salinization at a sidehill seep and closed basin in southern Alberta. Can J Soil Sci 73(2):209–222

Millington, RJ, Quirk, JP (1961) Permeability of porous solids. Faraday Soc Trans 57:1200–1206

Morin KA (1990) Problems and proposed solutions in predicting acid drainage with acid-base accounting. In: Gadsby J, Malick J, Day S (eds), Acid mine drainage: designing for closure. BiTech Publishers, Vancouver, pp 93–109

Nichol CF, Froese K, Sharma JS, Barbour SL (2016) Effects of oxidation on residual shear strength of shales within Lea Park Formation. Can Geotech J 53(12):1952–1964

Nordstrom DK (2011) Hydrogeochemical processes governing the origin, transport and fate of major and trace elements from mine wastes and mineralized rock to surface waters. Appl Geochem 26(11):1777–1791

Olatuyi SO, Leskiw LA (2014) Long-term changes in soil salinity as influenced by subsoil thickness in a reclaimed coal mine in east-central Alberta. Can J Soil Sci 94(5):605–620

Price WA, Errington J, Koyanagi V (1997) Guidelines for the prediction of acid rock drainage and metal leaching for mines in British Columbia: part I—general procedures and information requirements. In: Proceeding, 4th international conference on acid rock drainage (ICARD), Vancouver, BC, pp 1–14

Rhoades, JD (1982) Soluble salts. In: Page AL, Miller RH, Keeney DR (eds), Methods of Soil Analysis. Part 2, American Soc of Agronomy, Madison, WI, Agronomy Monograph no. 9, 2nd edit, pp 167–178

Sihota NJ, Mayer KU (2012) Characterizing vadose zone hydrocarbon biodegradation using carbon dioxide effluxes, isotopes, and reactive transport modeling. Vadose Zone J. doi:10.2136/vzj2011.0204

Sommerfeld, RA, Massman WJ, Musselman RC, Mosier AR (1996) Diffusional flux of CO2 through snow: spatial and temporal variability among alpine-subalpine sites. Global Biogeochem Cy 10(3):473–482

Spiers GA, Dudas MJ, Muehlenbachs K, Turchenek LW (1984) Mineralogy and oxygen isotope geochemistry of clays from surficial deposits in the Athabasca Tar Sands area. Can J Earth Sci 21(1):53–60

Sracek O, Choquette M, Gelinas P, Lefebvre R, Nicholson RV (2004) Geochemical characterization of acid mine drainage from a waste rock pile, Mine Doyon, Quebec, Canada. J Contam Hydrol 69(1–2):45–71

Steffen Robertson and Kristen Inc (1989) Draft Acid Rock Drainage Technical Guide—Vol 1. Prepared for the British Columbia AMD Task Force

van Stempvoort DR, Hendry MJ, Schoenau JJ, Krouse HR (1994) Sources and dynamics of sulphur in weathered till, western glaciated plains of North America. Chem Geol 111(1):35–56

Winston GC, Stephens BB, Sundquist ET, Hardy JP, Davis RE (1995) Seasonal variability in CO_2 transport through snow in a boreal forest. In: Tonnessen KA, Williams MW, Tranter M (eds), Biogeochemistry of seasonally snow-covered catchments. International Associatuion Hydrological Sciences, Wallingford, pp 61–70

Yanful EK, Bell AV, Woyshner MR (1993) Design of a composite soil cover for an experimental waste rock pile near Newcastle, New Brunswick, Canada. Can Geotech J 30(4):578–587